# Trial Embankment on Gold Mine Tailings

J.A.R. Ortigao, P. Paiva, A. Fahel, A. Landi, R. Souto

**Abstract.** This paper describes the behaviour of a 10 m high trial embankment built on silt gold mine tailings of Morro do Ouro Dam, Brazil. The dam is the country's largest tailings dam having 120 m in height and 4 km in length. This trial aimed at investigating tailings strength behaviour, which field experience has already indicated to be better than predicted by in situ and laboratory tests. The embankment foundation was instrumented with piezometers, settlement plates, profiler and inclinometers. Just after placing the first 2 m embankment layer, one observed water surges, interpreted as static liquefaction taking place at low stress level. Large porepressures and displacements were recorded during construction. The embankment height was taken to 10 m, much higher than predictions based on in situ and laboratory tests. The foundation strength was also analysed.

**Keywords:** tailings, trial embankment, liquefaction.

## 1. Introduction

How to obtain the shear strength of mine tailings for the design of a hundred metres high tailings dam?

Engineers at RPM Rio Paracatu Mining (now Kinross), Minas Gerais, Brazil, faced this challenge by means of a comprehensive approach employing in situ, laboratory testing and a full scale trial embankment, described in this paper.

This mine produces about 6 tonnes/year of gold and 17 to 22 Mtpa (million tonnes per annum) of tailings. A large expansion project took place between 2005 and 2008 to increase production to 30 Mtpa of tailings. Another tailings dam is currently under construction.

Mine tailings are disposed at the Morro do Ouro Dam, whose current dimensions are 120 m high and 4 km long, the country's largest tailings dam.

The dam project started some 30 years ago and the same Brazilian designers have been involved since the start and continue their work to date. This has been pointed out by the international design reviewer's board, as a safety measure in a long time project, as the project history is well known.

Dam safety is analysed every year by local and international consultants, with at least three hierarchy reviewers' levels above the designers. This has been very important for the successful history of this project, as all safety measures - including this trial embankment - deserve attention by the reviewers, designers and mine managers.

Morgenstern (2002) reviewed the dam design and site investigation results and recommended a low value in the order of 0.08 to 0.12 for the tailings undrained strength index ($c_u/\sigma'_{vo}$). This value is lower than the one given by undrained triaxial tests and piezocone analyses, which are in the order of 0.20 to 0.22.

Nevertheless, field experience from building dykes and access roads on the tailings demonstrated that failure is rare. Therefore, actual tailings shear strength looked well above what is predicted by in situ and laboratory tests.

One way to shed light on this dilemma was to build a trial embankment section on the tailings. This approach has been is use on soft clays in Brazil (Ortigao *et al.*, 1983; Ortigao, 1991) and overseas by many researchers (*e.g.*, Leroueil, *et al.*, 1985, 1990; Hunter & Fell, 2003). Nevertheless, there are only a few documented case histories of trial embankments tailings, apart from the Canadian liquefaction experiment programme CANLEX (Byrne *et al.*, 2000; Wride *et al.*, 2000).

Such a full-scale trial would lead to a better understanding of tailings behaviour and savings in further stages of the Morro do Ouro Dam.

This paper summarises tailings properties, describes the experiment, presents factual instrumentation data and stability analyses.

## 2. Trial Embankment Design

The trial embankment was located at the back of the tailings lake, far from the dam, and about 500 m from the tailings discharge point.

The test section dimensions (Figs. 2, and 3) were: 10 m in height with a front slope 1.5:1 and a gentle slope in the back. At this height, the foundation would have failed, according to predictions based on strength from laboratory and in situ tests. The top of the embankment was 30 m long, so that approximately plane strain conditions apply.

J.A.R.Ortigao, PhD, Terratek Ltd, Av Érico Veríssimo 901/302, 22621-180 Rio de Janeiro, RJ, Brazil. e-mail: ortigao@terratek.com.br.
P Paiva, Civil Engineer, Geo HydroTech Consultants Ltd, São Paulo, SP, Brazil, e-mail: ppaivafk@uol.com.br.
A Fahel, PhD, Samarco Mining, Formerly Geotechnical Consultant, Mariana, MG, Brazil. e-mail: andre.fahel@samarco.com
Antonio Landi, BSc, Mining Engineering, Kinross Mining, Belo Horizonte, MG, Brazil. e-mail: landi.borges@gmail.com.
Romulo Souto, Civil Engineer, Yamana Gold, formerly at Kinross RPM Mining, Jabobina, BA, Brazil. e-mail: romulo.souto@yamanagold.com.
Submitted on May 18, 2011; Final Acceptance on February 14, 2013; Discussion open until August 30, 2013.

**Figure 1** - Morro do Ouro tailings dam.

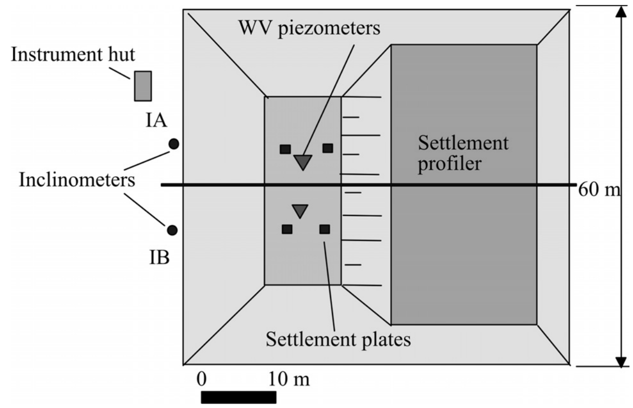


**Figure 3** - Plan view, test embankment.

**Figure 4** - Embankment at 5 m height.

The foundation instrumentation included: electrical vibrating wire piezometers, settlement plates, a settlement profiler and inclinometers.

The loading rate was as fast as possible, to match the worst loading conditions and maximum porepressures build-up. The final height was reached in just seven days. Earthworks took place around the clock, 24 h a day.

Figures 4 to 6 show the embankment under construction and at the end of the project.

## 3. Tailings Properties

Previous studies and laboratory tests indicate that Mina do Ouro tailings is a soft dark grey silty material having 15% of clay size particles and about 60% silt.

Atterberg limits are: liquid limit LL is 28%, plasticity index PI = 4%, water content w = 50% and average unit weight $\gamma$ = 17.4 kN/m$^3$.

### 3.1. Laboratory triaxial tests

Stress-strain-strength assessment was carried out through load controlled $K_0$-consolidated undrained triaxial compression tests (CK$_0$U-C tests) on reconstituted samples of varying densities. Only the loose state, corresponding to a dry unit weight of 8 kN/m$^3$, will be presented here.

Specimens were moist tamped in four soil layers in the triaxial mould until the desired density and void ratio was achieved. Saturation, then, took place by water seepage over 12 hours, followed by back-pressuring in small 25 kPa stages until reaching a minimum of porepressure parameter

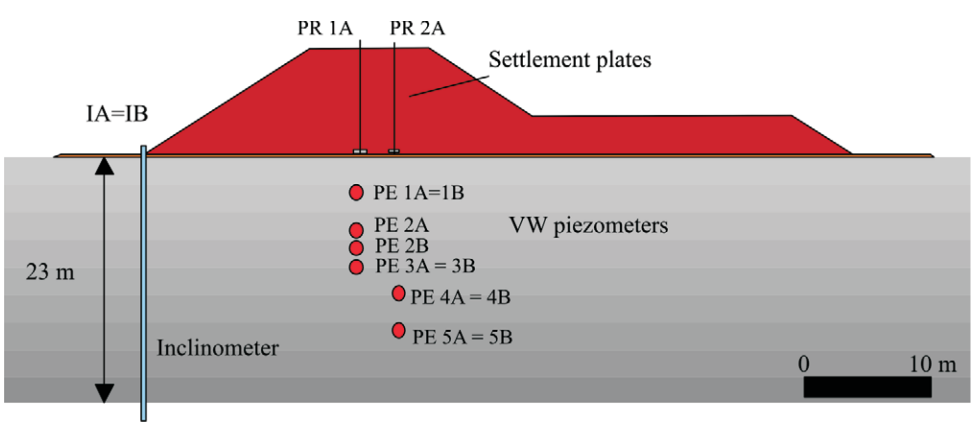


**Figure 2** - Cross section of the test embankment.

**Figure 5** - Access road.

**Figure 6 -** Finished embankment.

$B$ of 0.97. Shear was then applied by a static loading frame by increasing deviator stress in controlled increments.

Figure 7 presents stress-strain and porepressure behaviour of loose specimens. The co-ordinates are $p' = (\sigma'_1 + \sigma'_2 + \sigma'_3)/3$, $q = \sigma_1 - \sigma_3$ and void ratio $e$. The confining stress levels varied from 25 to 200 kPa.

Figure 8 shows the $p'$: $q$: $e$ plot. The specimen under 200 kPa confining stress shows little deformation under 1% strain, followed by large deformation and porepressure rise tending to reach failure under constant stress.

The stress paths enable the definition of a CSL (critical state line), which present a friction angle of $\phi' = 32^{\circ}$.

The $p'$: $e$ plot yields the following approximate equation for the CSL: ($p'$ in kPa).

$$e = 2.3 - 0.5 \log p'$$

All tests enable the definition of an intermediate line between the $K_0$ and the CSL, whose deformation magnitude and rate seem to increase by a large amount. This line has been named either instability or collapse line.

The loose specimens at lower confining stresses show a peak strength value followed by very high deformation, which leads to failure. This is typical of static liquefaction behaviour under low confining stress, which presents strong strain-softening under low confining stress that can be detected under strain-controlled tests (Yamamuro & Lade, 1997 and Yamamuro & Covert, 2001).

As confining stress increases, the strain softening tends to decrease and eventually the loose tailings show strain-hardening, as in the loose specimen tested at 200 kPa confining stress.

The undrained strength ratio at ($c_u/\sigma'_{vc}$) can be taken at the point where the stress path crossed the instability line, which leads to $c_u/\sigma'_{vc} = 0.2$.

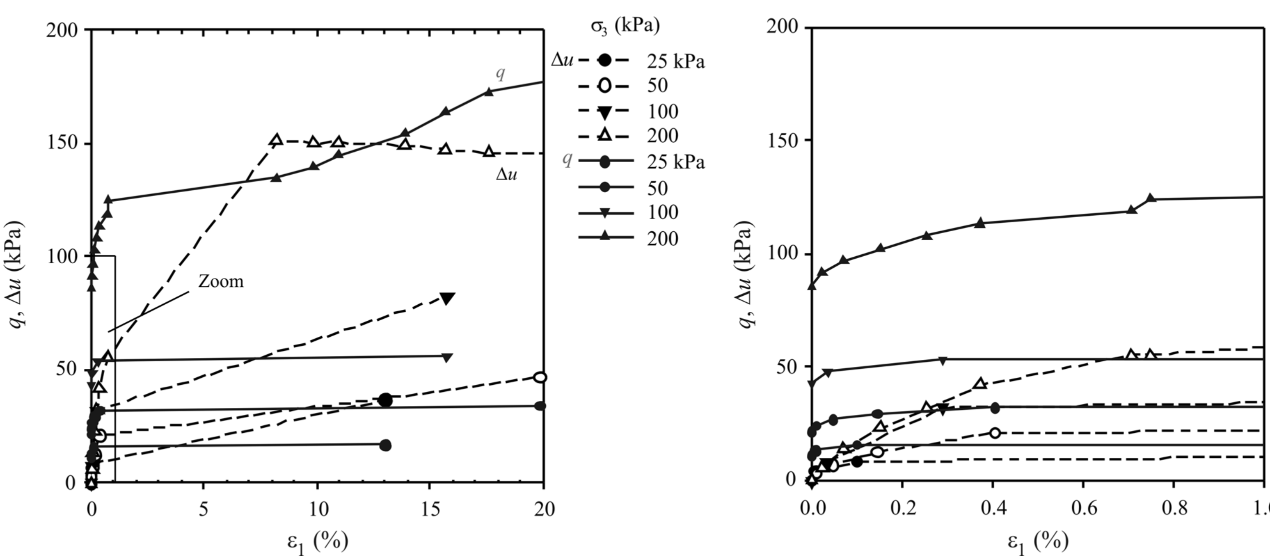


**Figure 7** - Stress-strain and porepressure behaviour, loose specimens (left normal view, right zoomed view).

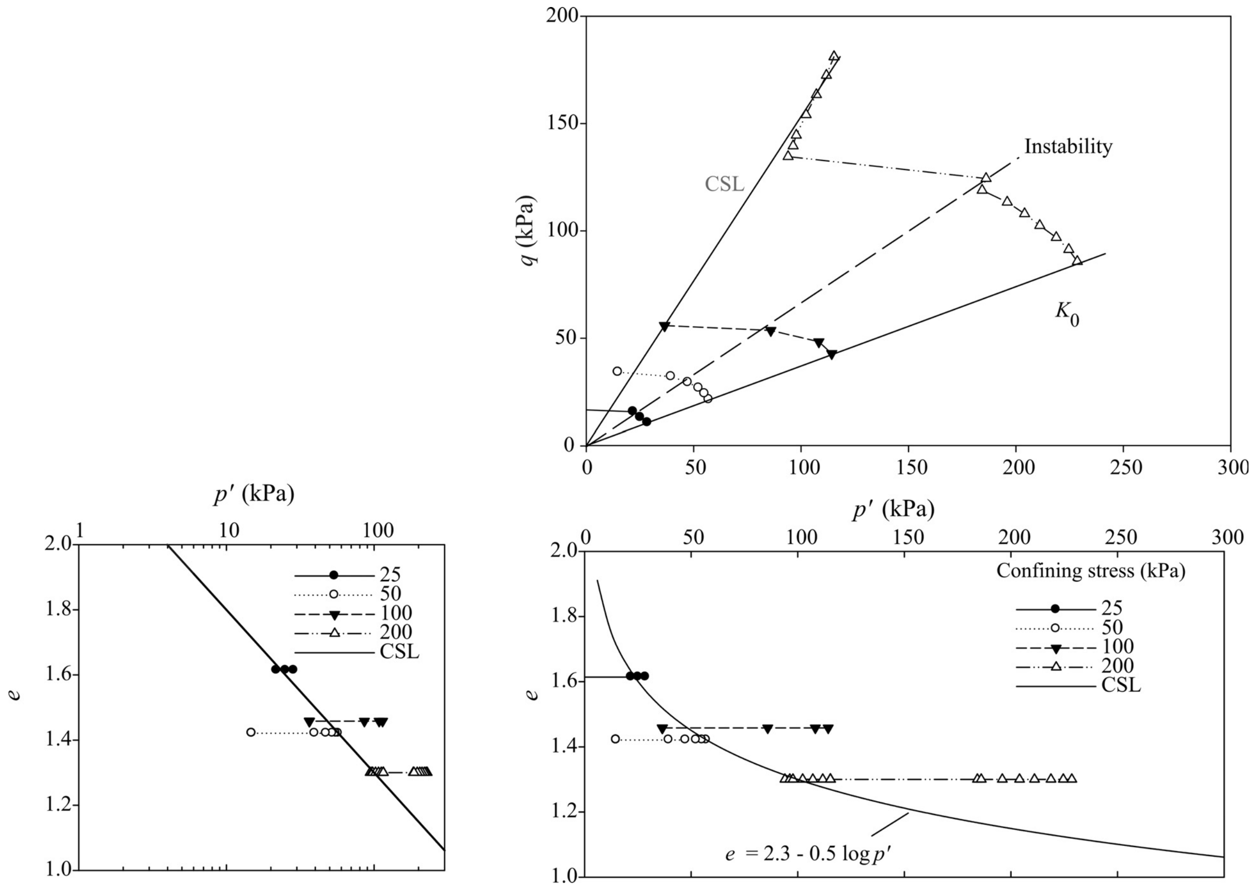


**Figure 8** - Stress paths, loose specimens.

### 3.2. In situ tests

The tailings site investigation programme included some 15 seismic piezocone tests (CPTUS).

Figure 9 shows a typical result of a test carried out close to the trial embankment site. It presents plots of tip resistance $q_t$; friction ratio, $R_f$ , porepressures $u_2$ and hydrostatic $u_0$, $I_c$, the Soil Behaviour Type or SBT index (Robertson, 2012). Figure 10 shows the normalised CPT parameters for the tip resistance, $Q_{tn}$, local friction, $F$, and porepressure $B_q$ described elsewhere (*e.g.*, Robertson, 2012).

The tip resistance through the upper uncompacted embankment fill is greater than 1 MPa down to 12 m depth and then decreases in the tailings below. The friction ratio $R_f$ lies in the range 2 to 4% in the fill and then increases in the tailings to values above 8%. This plot also shows a decrease in $R_f$ below 27 m depth, which is an indication of increase in sand content.

The porepressure $u_2$ in nearly nil in the fill, but reaches high values in the tailings, well above $u_0$. The porepressure parameter $B_q$ increases dramatically in the tailings just below the fill and reaches values of above 1. Porepressure dissipation rate in the tailings is so high that full dissipation is achieved during the short time spent at adding steel rods. This is the cause of the zig-zag in the $u_2$ plot of all boreholes.

Porepressure dissipation rates are very fast yielding a coefficient of consolidation from 3000 to 4000 m$^2$/ year, *i.e.*, about 800 times a typical soft sedimentary clay (taken as 5 m$^2$/year, *e.g.*, Ortigao, 1995). This raises the argument that a partial drained behaviour could be assumed for the tailings, especially if loading rate is slow.

Figure 11 shows $q_t$ and shear wave velocity $V_s$ profiles close to the dam crest closer to the trial embankment site. Lower $q_t$ values at tests at the back of the pond, far away from the dam, is because they are closer to the tailings discharge point at the back of the tailings. The CPTUS closer to the dam has a 18m thick fill at the top. On the other hand, the one at the trial embankment site has just 5 m of fill. $V_s$ values are in the range of 100 to 200 m/s in the tailings.

### 3.3. Flow liquefaction assessment from CPTU

This section looks at flow liquefaction using recent work by Robertson (2009, 2010), who updated a previous method (Robertson & Wride, 1998). Shuttle & Cunning (2007) discussed Robertson and Wride's method limitations. The work presented here is based on an updated version of the original Robertson and Wride's method (1998), details of which were given in Robertson (2008, 2010)

This updated method takes into account cyclic softening and evaluates post liquefaction undrained strength ratio based on case histories recorded by Olson & Stark (2002, 2003).

Robertson's (2010) method consists of obtaining the normalised CPT parameters for tip resistance (*Q*) and friction (*F*) and plotting the data as in the SBT chart as Fig. 12,

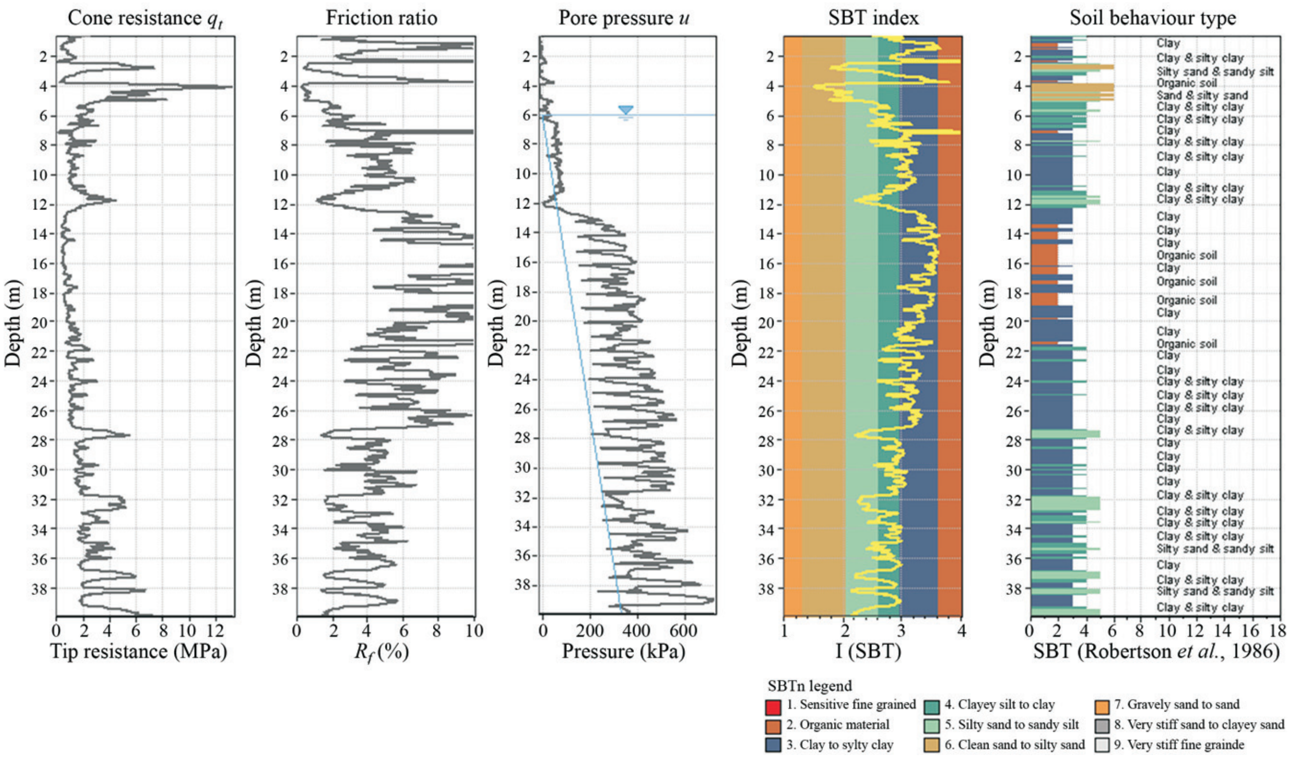


**Figure 9** - Typical CPTU results.

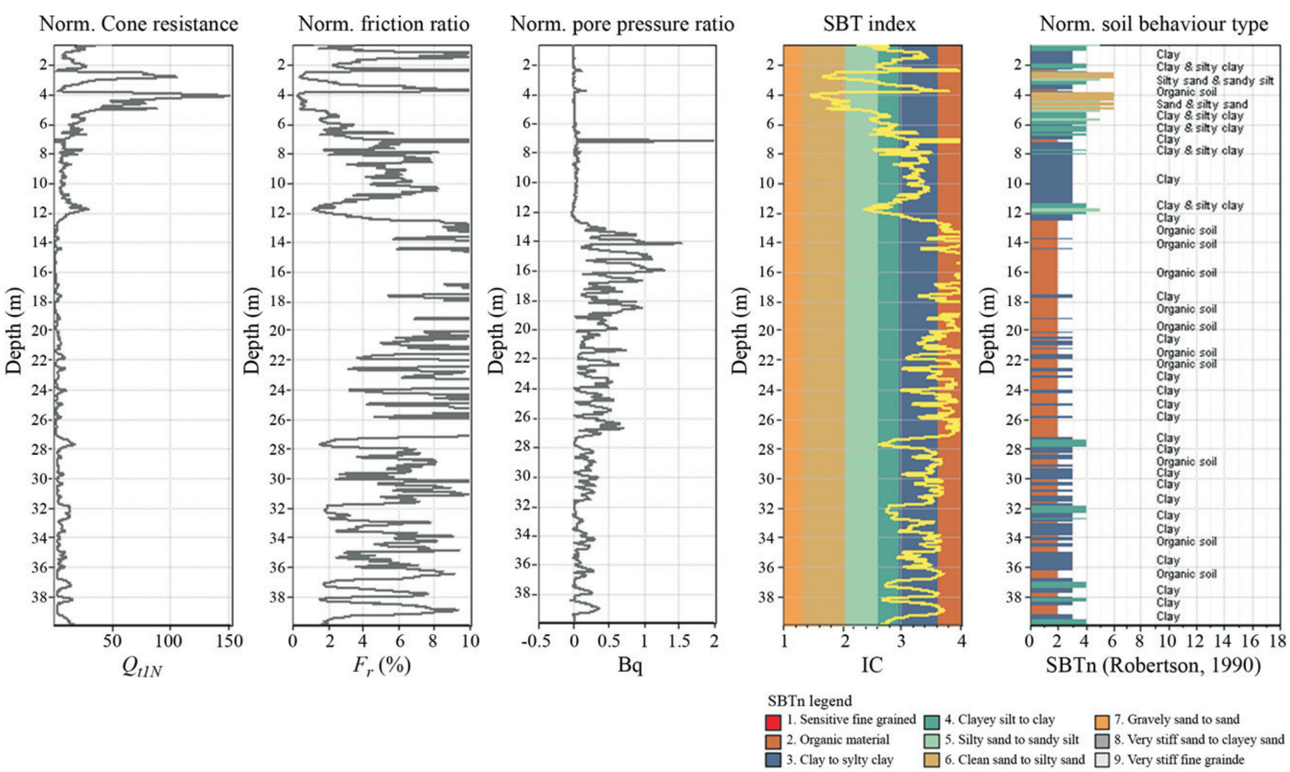


**Figure 10** - CPTU normalised results.

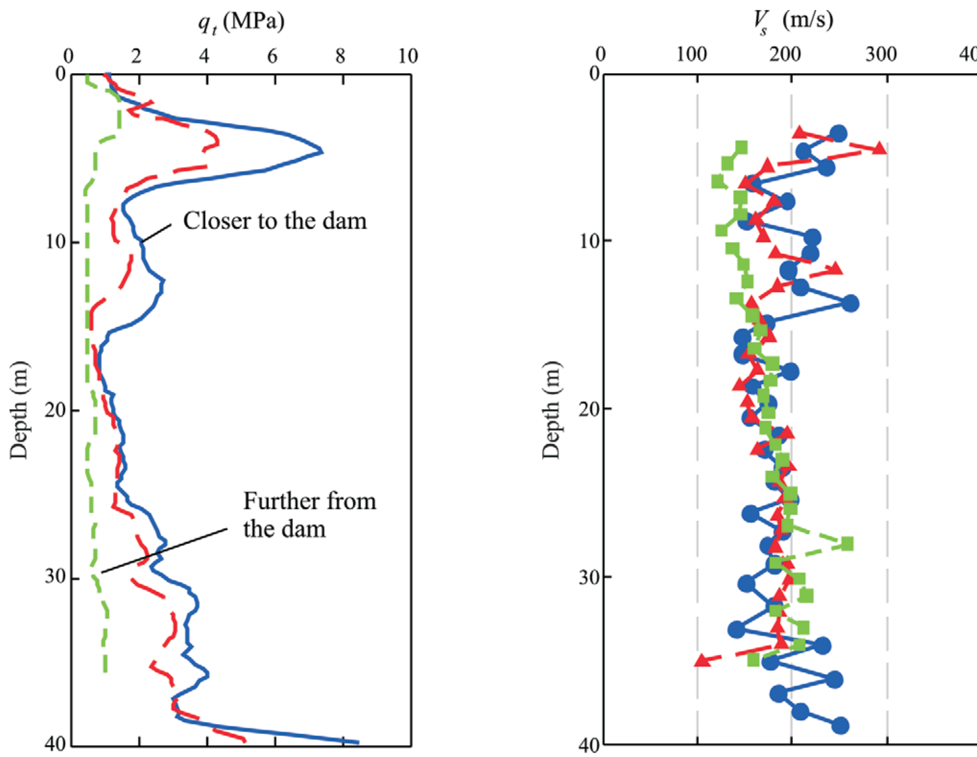


**Figure 11** - CPTUS seismic results as a function of the distance from the dam crest.

as done for these CPTU data. Zones $A_1$ and $A_2$ are the zones where cyclic and flow liquefaction are possible.

The next step is to plot the data in Fig. 13, which shows (a) the tip resistance, (b) $K_c$, a correction factor which depends on the grain characteristics, (c) and $Q_{tncs}$, the normalised tip resistance equivalent to a clean sand value (Robertson & Wride, 1998). $Q_{tncs}$ parameter values above 70 indicates contractive soils and correlates well with state parameter $\Psi > 0$ (Jefferies & Been, 2006). Figure 13 shows $Q_{tncs} > 70$ in the tailings, thus contractive behaviour takes place. On the right of Fig. 13 there is: (d) a plot of the pre and post liquefaction undrained ratio. The latter shows values as low as 0.1 in the tailings from 13 to 19 m depth.

## 3.4. Comparison between undrained strength predictions

This section compares undrained strength predictions from different methods, plotted in Figure 14, discussed as follows.

### *3.4.1. Olson and Stark's method*

Figure 14 plots undrained strength ratio and values for pre and post liquefaction from CPTU correlation proposed by Olson & Stark (2002, 2003). It yields the ratio corresponding to pre (or triggering) and post liquefaction conditions, yielding the following parameters:

$c_{uLiq}/\sigma'_{v0}$ = pre and post liquefaction undrained strength ratio to the effective overburden stress;

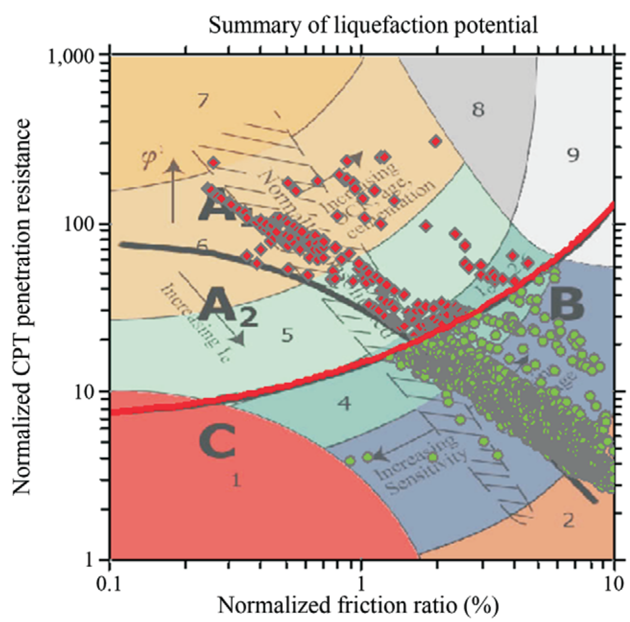


Zone A1: Cyclic liquefaction likely depending on size and duration of cyclic loading
Zone A2: Cyclic liquefaction and strength loss likely depending on loading and ground geometry
Zone B: Liquefaction and post-earthquake strength loss unlikely, check cyclic softening
Zone C: Cyclic liquefation and strength loss possible depending on soil plasticity, brittleness/sensitivity, strain to peak undrained strength and ground geometry

**Figure 12** - CPT x SBT - Soil Behaviour Type chart for liquefaction.

$c_{uLiq}$ = pre and post liquefaction undrained strength at the tailings (kPa).

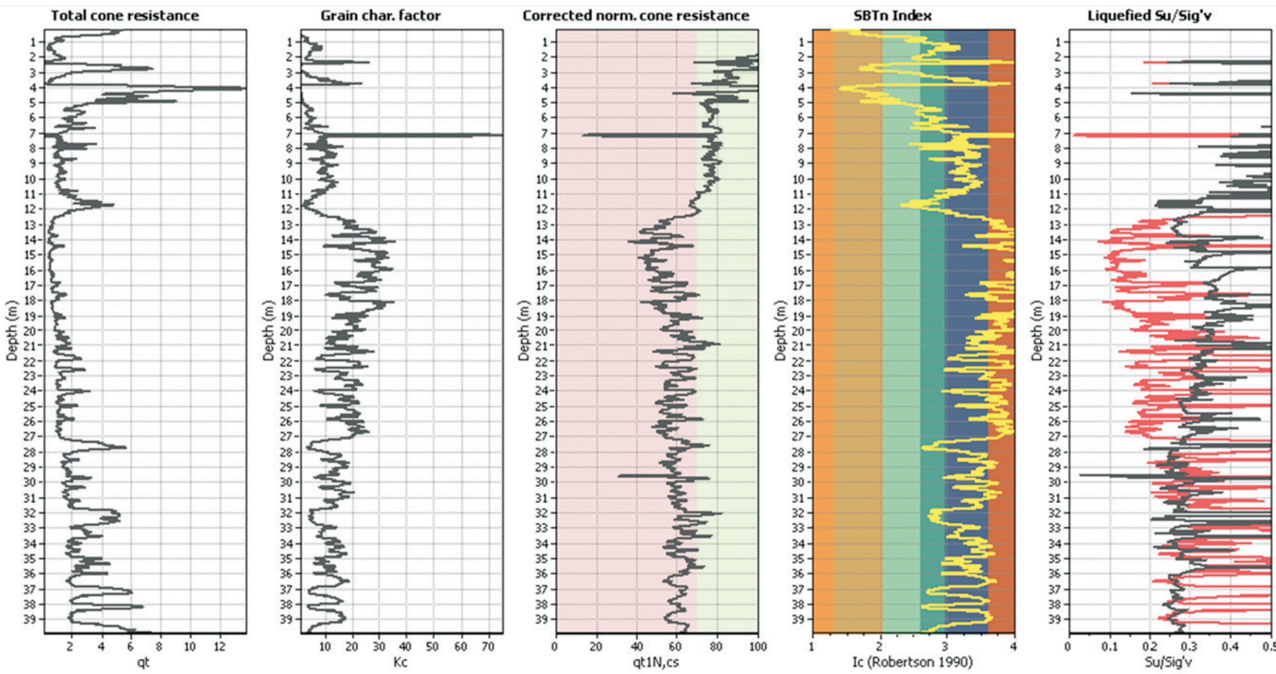


**Figure 13** - Flow liquefaction assessment, according to Robertson (2008, 2010).

*3.4.2. Jefferies and Been's CSSM*

Jefferies & Been (2006) book summarises their work on the application of CSSM (critical state soil mechanics) to understanding the behaviour of tailings and loose sands. They provide a useful spreadsheet to analyse CPTU data and this yielded post liquefaction or residual undrained values ($c_{ur}$) also plotted in Fig. 14, which yields very low values.

*3.4.3. $N_{kt}$ approach*

Figure 14 presents empirical values for the undrained strength based on $N_{kt}$ and compares with strength obtained by means of the equation:

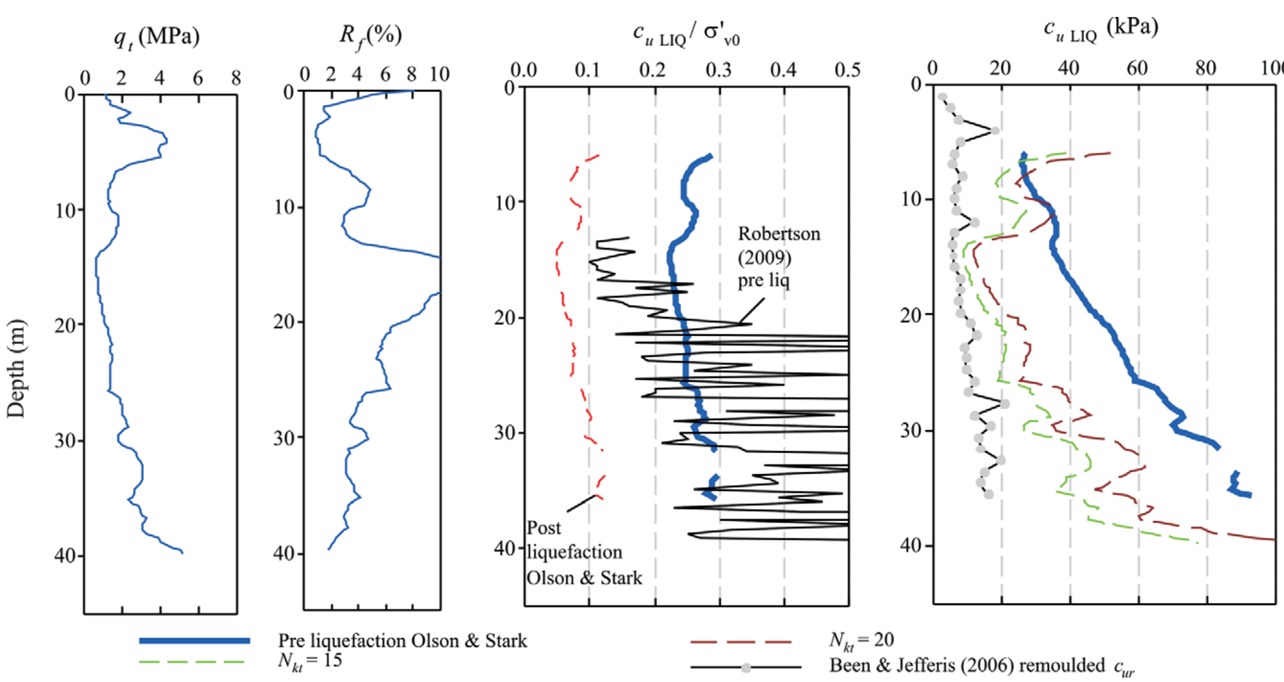


**Figure 14** - Comparison between undrained strength predictions: Olson & Stark (2003), Jefferies & Been (2006), $N_{kt}$ and Robertson (2010) methods.

$$c_u = \frac{q_t}{N_{kt}} \tag{1}$$

where $N_{kt}$ is an empirical coefficient. This work assumes $N_{kt}$ equals to 15 and 20, which is the range for most clays.

As discussed previously in this paper the instability or collapse line yields the undrained strength ($c_u/\sigma'_{vc}$) ratio of 0.2, which is just in between Olson and Stark's results (Fig. 14).

## 4. Embankment Construction

The borrow material was a residual silt from a nearby area, ripped by dozers from the top soil to a depth of about 1.5 m. The embankment was about 100 m from the beach on the top of a minimum of 20 m thick tailings. An access road was built from the borrow pit to the embankment location.

A 400 g/m$^2$ non-woven geosynthetic was placed over the entire area (Fig. 15), followed by a 80-90 cm thick embankment layer. The geosynthetic aimed at improving and reducing thickness of the first layer, which was the minimum necessary to allow dozers and lorries to operate. However, this first layer led to high initial settlements on the soft tailings. Boreholes carried out through this first layer indicated that the total fill thickness was about 2 m, therefore, the initial settlement was about 1.1 to 1.2 m.

Light dozers, D4 type, spread the fill material. After this work platform was in place, construction stopped to allow instrumentation installation and initial or baseline readings. This phase took about one month.

### 4.1. Loading rate

Figure 16 presents the time-history of embankment loading. It was the fastest possible rate under given conditions of the embankment dimensions, distance to the borrow pit and earthwork equipment.

Earthworks took place around the clock, 24 h a day, with one hour breaks for changing shifts at 6:00 and 18:00 h. Other breaks occurred at 12:00 and 24:00 h for meals.

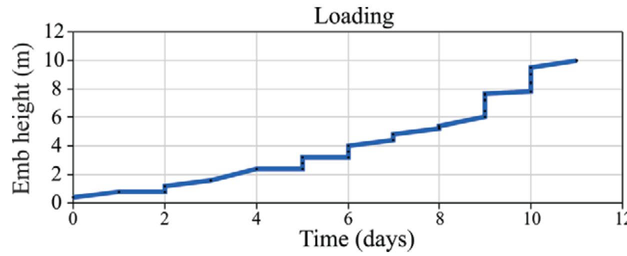


**Figure 16** - Embankment loading rate.

The initial rising rate was slow, as the spreading area was too large, and it took two days to reach 2 m in height, and another two days to reach the level of the berm. From this point, the rise was fast, and the embankment reached 10 m height in only six days.

### 4.2. Liquefaction

Just after placing the first embankment layer, evidence of liquefaction took place. Figures 17 to 20 present photographic records of the events. Firstly, a small water spring or *sand boil* surged on the top of the embankment and continued until forming a "volcano" of tailings, about one metre in diameter. This phenomenon took place only under the first embankment layer.

Indeed, static liquefaction seems to have occurred under very low confining stress only. Laboratory evidence supports this conclusion, as loose specimens at low confining stress showed very large deformation after instability or collapse, with a considerable rise in porepressures.

### 4.3. Instrumentation

The instrumentation consisted of ten vibrating wire (VW) piezometers in the foundation, two inclinometer access tubes at the embankment toe, a hydraulic settlement profiler along the base of the main cross-section and four

**Figure 15** - Placing the geosynthetic on the tailings.

**Figure 17** - Sand boils on the top of the first layer.

**Figure 18** - Sand boils on the top of the first embankment layer.

**Figure 19** - Sand boils.

**Figure 20** - Sand boils, zoomed view.

settlement plates. A benchmark was installed on firm ground close to the borrow pit area and an observation well close to the embankment.

The VW piezometers were installed in *H* size (100 mm diameter) boreholes into a one-metre high sand bulb and sealed with 0.5 m thick seal of bentonite balls followed by filling with bentonite mud to the top of the borehole.

Electrical cables were extended in shallow trenches to the instrument hut located in front of the embankment. A portable read-out unit read the piezometers both during installation and after construction. A data acquisition system installed in the instrument hut read piezometer data during construction at regular intervals of about half an hour.

Inclinometer access tubes 80 mm in diameter were installed in *P* size (150 mm) holes drilled a few metres into firm ground, beyond the tailings bottom-line. A bentonite-cement grout filled the annular space between tubes and borehole wall. They were surveyed with a digital inclinometer probe.

A 50 mm diameter access steel tube was placed in a shallow trench along the embankment cross section, and backfilled. This tube was surveyed regularly with a hydraulic settlement profiler which slides in the access tube, providing settlement readings at 5 m intervals. This unit consisted of an electrical VW low pressure transducer connected to a constant level water reservoir outside the embankment. The system enables atmospheric pressure and temperature corrections. The overall accuracy is about ± 5 mm.

Four settlement plates were installed. Their protruding rods spoil earthworks, however, they are very important for post-construction monitoring. They were surveyed with an engineer's level relatively to the benchmark.

The field crew took inclinometer and settlement profiler readings twice a day during changing shifts at 6:00 h and 18:00 h. Settlement plates were read once a day at noon. Piezometers were read nearly continuously.

The field crew carried out baseline readings, field calibration and redundant checking of all instruments before and after installation for over a fortnight before embankment construction started. Readings were also obtained by RPM crew with a second VW readout box and inclinometer probe. This ensured the high data quality needed for this experiment.

Settlement and porepressure readings continue for post-construction monitoring, although these data will be analysed in another paper.

### 4.4. Observations during construction

The first fill layer led to a settlement of about 1.1 to 1.2 m, which was not taken into account in the calculations.

The observation well indicated that the water table coincided with tailings surface. This instrument was located too close to the embankment toe, and showed porepressure rise during loading. This report assumed that the ground water remained unchanged through the experiment.

When the embankment reached 5 m in height, the tailings surface on the lakeside of the embankment showed signs of bulging. Inclinometers and piezometers also recorded jumps at the same time, and will be discussed later. This was, then, interpreted as a local failure at that stage.

At the end of loading, the embankment was thoroughly inspected and presented no visible signs of failure or cracking.

## 5. Instrumentation Results

### 5.1. Porepressures

Figures 21 to 28 summarise porepressure measurements in separate plots for vertical A and B, showing that porepressures built up considerably during loading.

Figures 21 and 22 present excess porepressures $\Delta u$ *vs.* time and embankment height.

Figures 23 and 24 plot excess porepressures $\Delta u$ during loading as a function of total vertical stress increment $\Delta\sigma_v$, which is the increase in overburden stress $\Delta\sigma_v = \gamma H$ due to the embankment loading. The rate of porepressure build-up is higher in the initial phase until the embankment reached 6 m in height, and then decreases slightly. This could be the influence of dissipation rate.

One can observe a sharp drop in porepressures when the embankment reached about 5 m in height, followed by a recovery with loading. This was accompanied by a jump in horizontal displacements measured by the inclinometers, which will be discussed later. Ortigao *et al.* (1983) observed a similar porepressure decrease during failure of a test embankment on soft clay. This can be explained by local yielding due to dilation taking place close to piezometer sensors.

The plots of $\Delta u$ *vs.* $\Delta\sigma_v$ include a $\Delta u = \Delta\sigma_v$ line, which corresponds to fully undrained case of porepressure increase. Piezometers located close to the centre of the tailings layer show higher porepressures and they plot closer to this line, whereas those close to the top plot well below this line, due to porepressure dissipation.

Figures 25 and 26 present porepressure isochrones. Instruments in the centre of the tailings layer show larger porepressures than those close to the top. This is a typical phenomenon caused by faster dissipation closer to drainage boundaries.

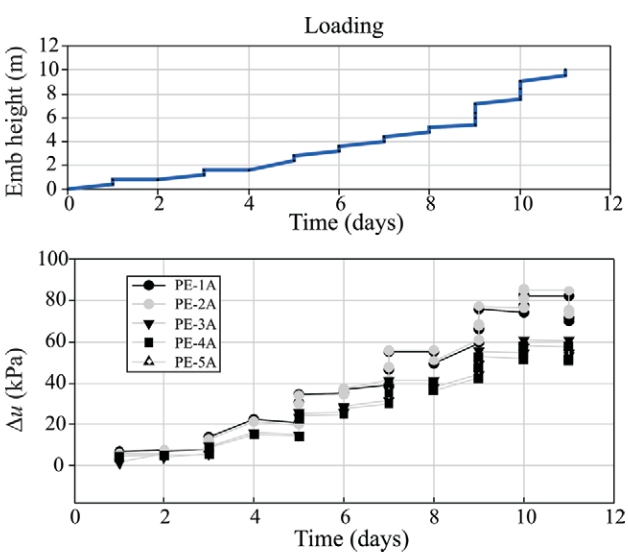


**Figure 21** - Porepressures during loading, vertical A.

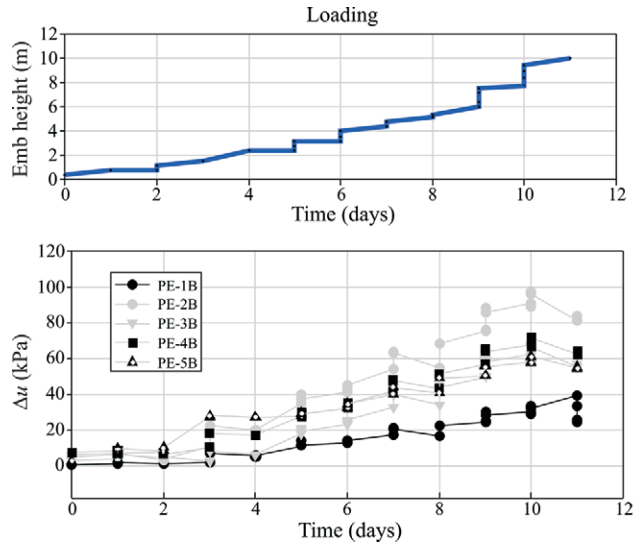


**Figure 22** - Porepressures during loading, vertical B.

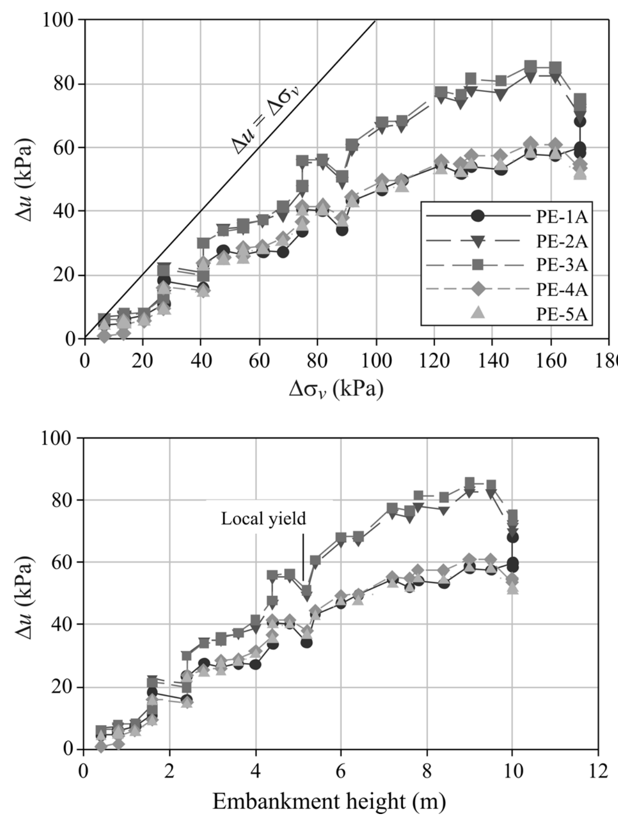


**Figure 23** - Excess porepressures during loading, vertical A.

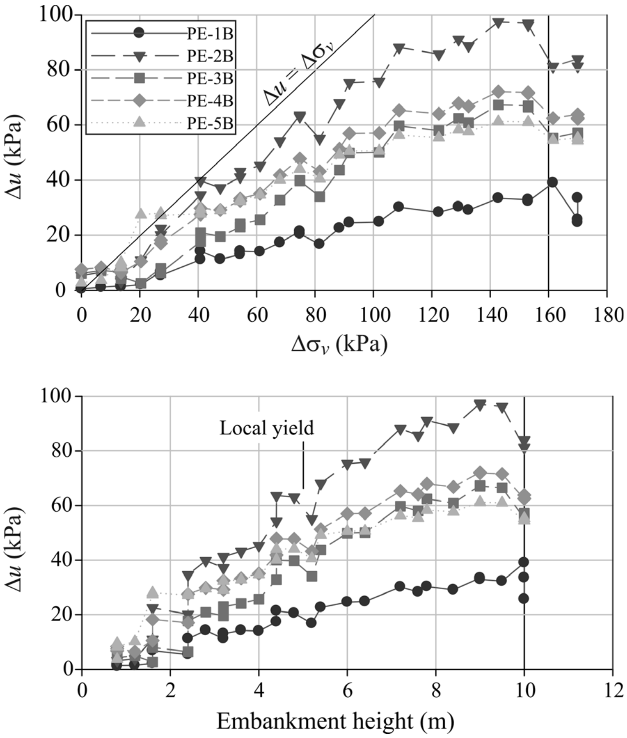


**Figure 24** - Excess porepressures during loading, vertical B.

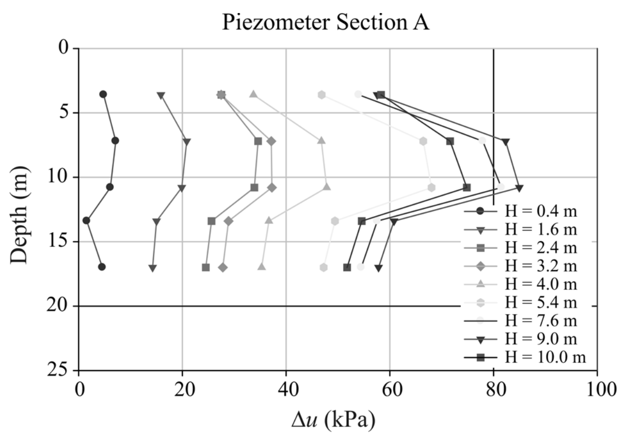


**Figure 25** - Porepressure isochrones, vertical A.

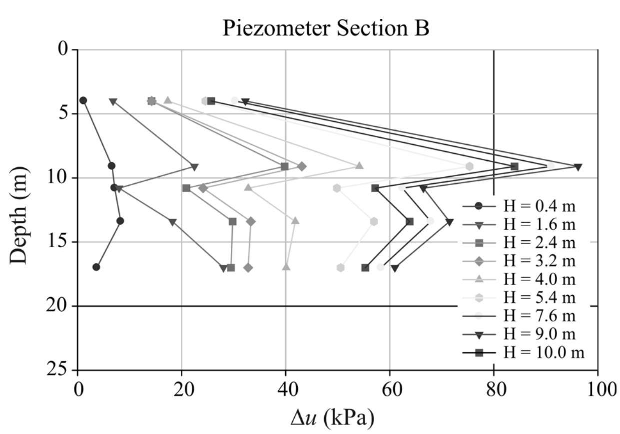


**Figure 26** - Porepressure isochrones, vertical B.

Porepressure isochrones are re-plotted in Figs. 27 and 28, presenting normalised porepressure parameter $B = \Delta u/\Delta\sigma_v$ *vs.* normalised depth $z/D$, where $D$ is the depth of the tailings. These plots demonstrate that the measured porepressures follow the typical behaviour observed in a number of cases of loading on soft clay, where partial dissi-

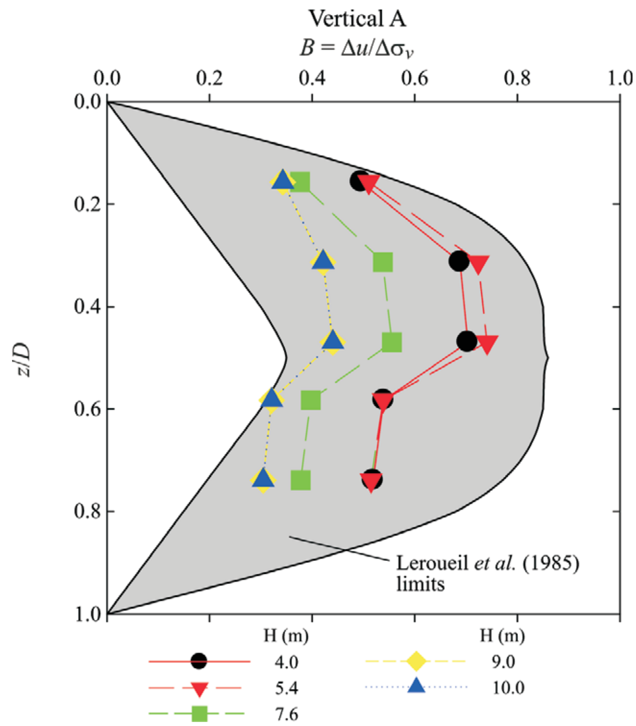


**Figure 27** - Porepressure parameter B, vertical A.

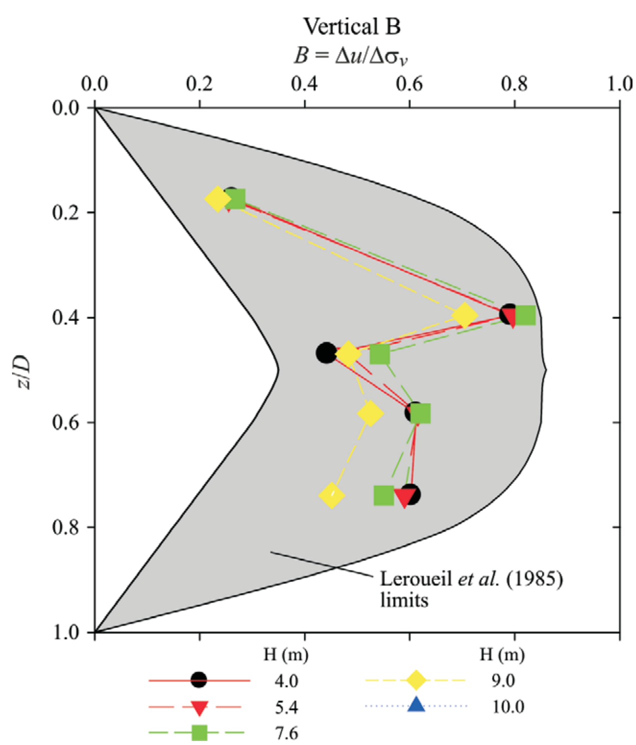


**Figure 28** - Porepressure parameter B, vertical B.

pation takes place. Leroueil *et al.* (1985) observed this phenomenon in a number of cases in soft clays, when the clay is still at the overconsolidation stress range. Indeed, measurements at this test embankment fall within the limits proposed by these authors, also observed for other Brazilian soft clays (Ortigao *et al.*, 1983).

### 5.2. Porepressure dissipation after construction

Figure 29 presents porepressures *vs.* time for piezometers under vertical A, showing fast dissipation rates after construction, which took 10 days to achieve complete dissipation. This figure also plots results from a very simple one-dimensional Terzaghi dissipation model. The coefficient of consolidation was varied until an agreement was obtained, leading to the value of this coefficient in the vertical direction of $c_v = 4000 m^2/year$.

It is interesting to compare this value with the coefficient of consolidation in the horizontal direction ($c_h$) from many piezocone dissipation tests in the tailings. Figure 30 is a histogram of CPTU data and includes the back-figured value from the trial embankment dissipation. The results are in good agreement, showing that $c_v$ and $c_h$ values are very close for the tailings. This also shows that the piezocone dissipation radial model is a good approximation to the test, as well as, the simple vertical 1D consolidation model. Additionally, the tailings show homogeneous permeability behaviour.

### 5.3. Inclinometer measurements

Figures 31 to 35 present horizontal displacements measure with inclinometers at the toe. The plots in Figs. 31, 32 and 33 present calculated displacements and change of

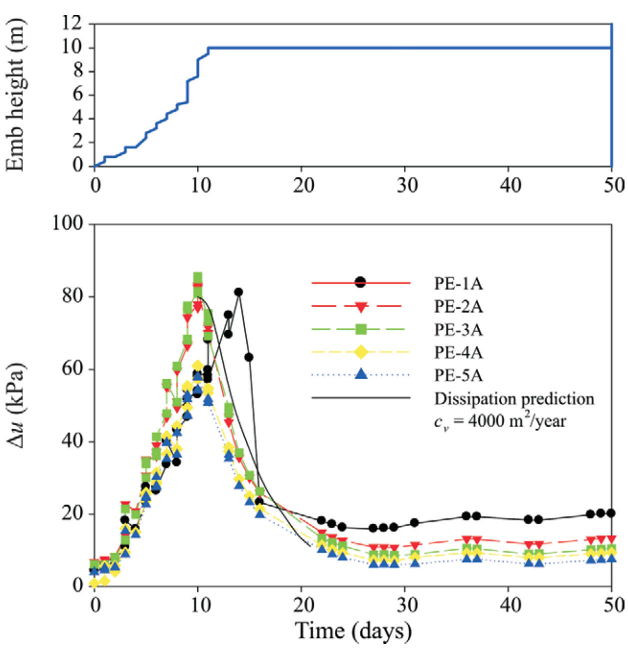


**Figure 29** - Porepressure dissipation after construction, vertical A.

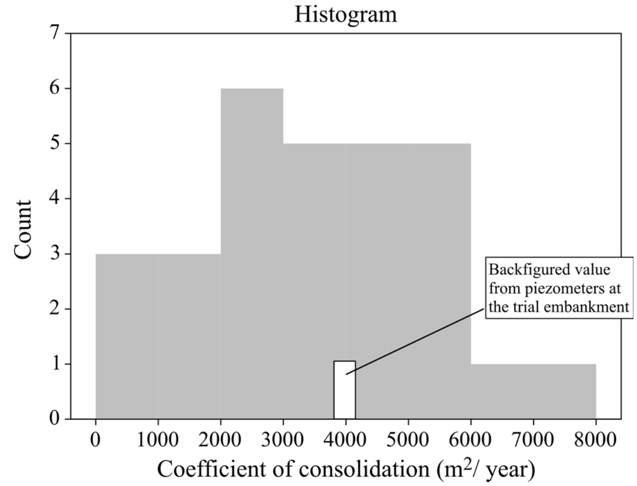


**Figure 30** - Coefficient of consolidation from piezocone and piezometer dissipation.

readings with depth for various heights. Maximum horizontal displacements are about 150 mm and 110 mm at 7 m depth in inclinometer IA and IB, respectively.

When the embankment reached 5 m in height these plots show a sharp jump in the deformation, consistent with local yielding also detected at the piezometers.

The change of readings is proportional to soil distortion. The largest value possibly indicates the location of a slip surface and is related to shear strain of soil, as discussed by Ortigao *et al.* (1983b). The measurements show large distortions at 15 m depth, with consistent results in both tubes.

Measurements at the two access tubes show similar results on axis *A* (main axis, across the embankment), but quite different behaviour along the secondary axis *B*. Inclinometer IA presented negligible lateral displacements and the results are not included. On the other hand, considerable lateral spreading took place at inclinometer IB (Fig. 33). Maximum displacements were about 60 mm.

Figures 34 and 35 present horizontal displacements measured by the inclinometers and corresponding change of readings as a function of the embankment height.

The amount of angular deflection θ is obtained from the change in inclinometer readings (change), according to the following equation:

### 5.4. Settlements

Figure 36 presents recorded settlements *vs.* time and *vs.* embankment height. Figure 37 gives settlement results obtained by the settlement profiler. In both cases, the initial settlement caused by the working mat has not been included.

The maximum settlement at the end of construction was 800 mm in the settlement plates and about 700 mm in the settlement profiler. Certainly, the settlement plates give the correct result, while the profiler gives the shape. The reason is that, for very large settlements, corrections should

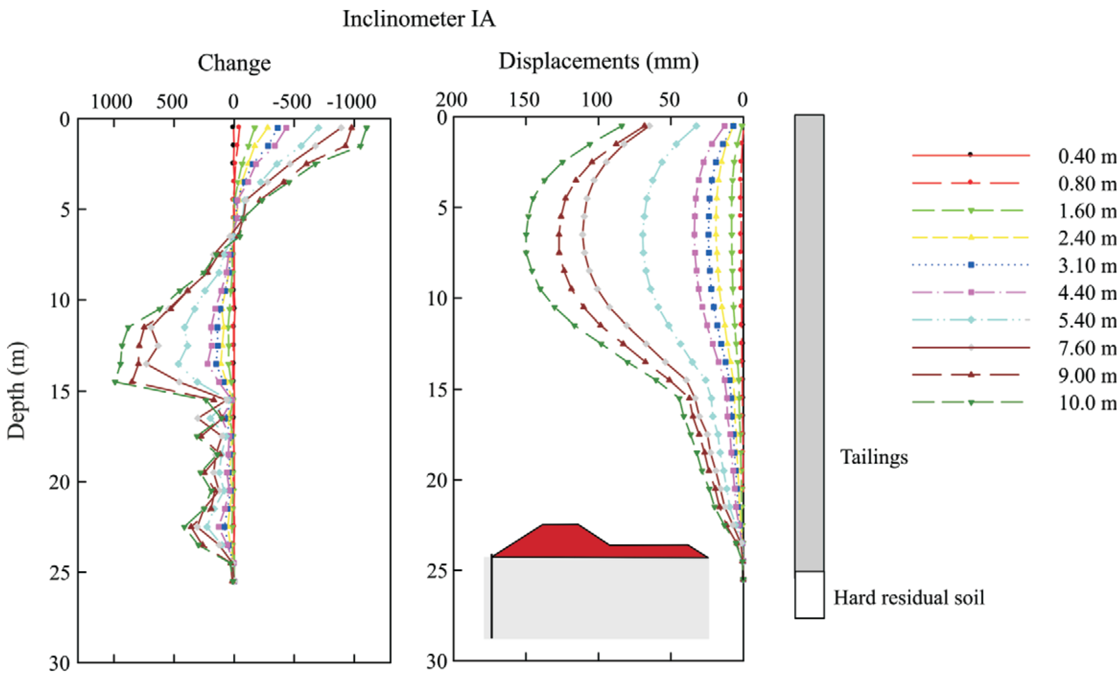


**Figure 31** - Inclinometer IA results.

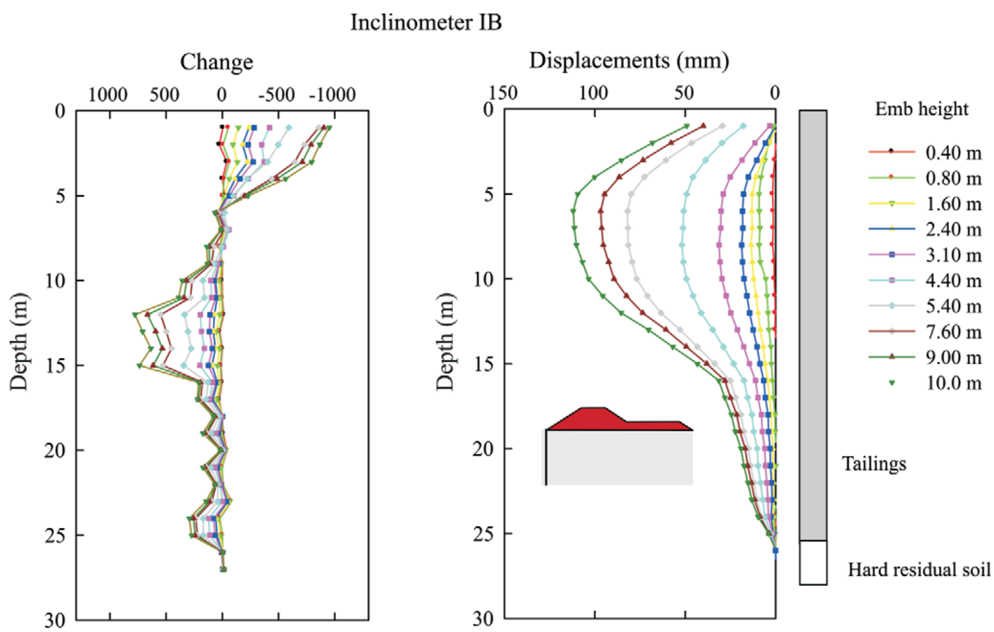


**Figure 32** - Inclinometer IB results, main axis.

be made for the curvature of the profiler, as the access tube deforms.

### 5.5. Horizontal displacements *vs.* settlements

Figure 38 presents a plot of maximum settlements *vs.* maximum horizontal displacements measured at the same embankment height. On the same figure there are dashed lines proposed by Leroueil *et al.* (1985) for drained and undrained behaviour, based on similar measurements at several embankments on soft clay. The trial embankment data in Figure 38 plot close to the drained behaviour line.

### 5.6. Prediction of impending failure from instrumentation results

This embankment shows very clearly that inclinometer results are very sensitive to impending failure. Plots of incli-

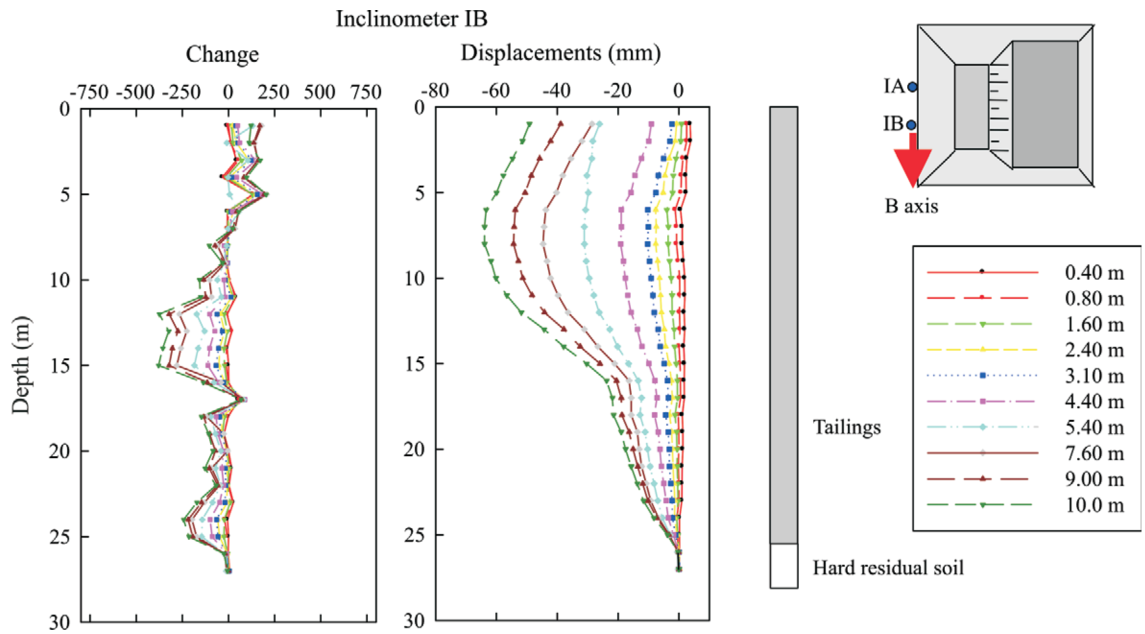


**Figure 33** - Inclinometer IB results, lateral axis.

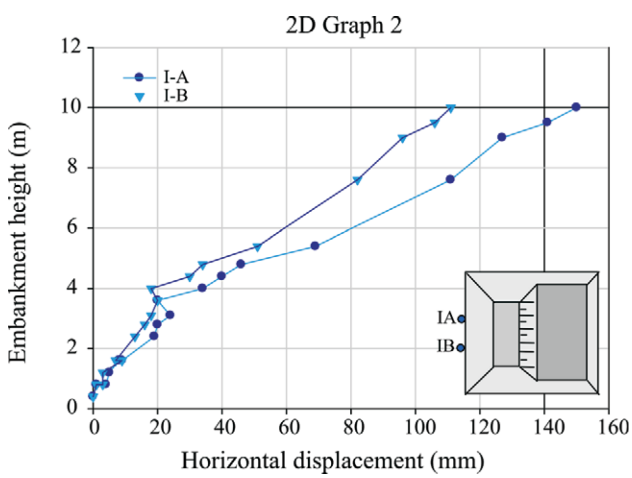


**Figure 34** - Horizontal displacements *vs.* embankment height.

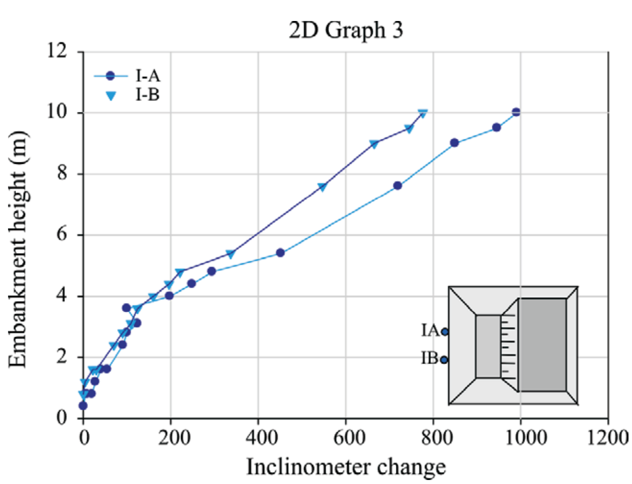


**Figure 35** - Inclinometer change of readings *vs.* embankment height.

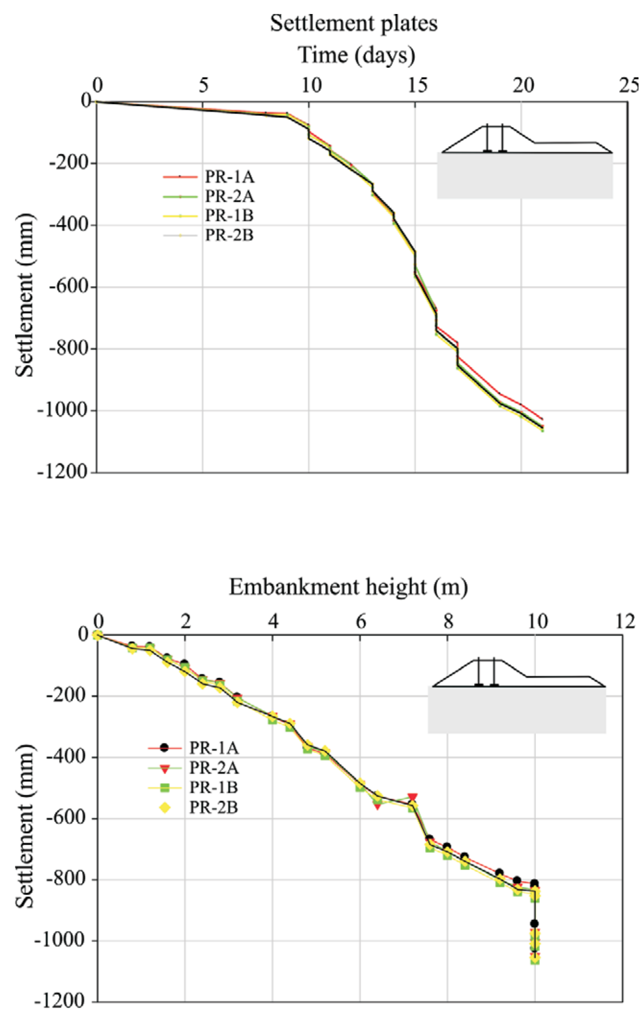


**Figure 36** - Settlement plates results.

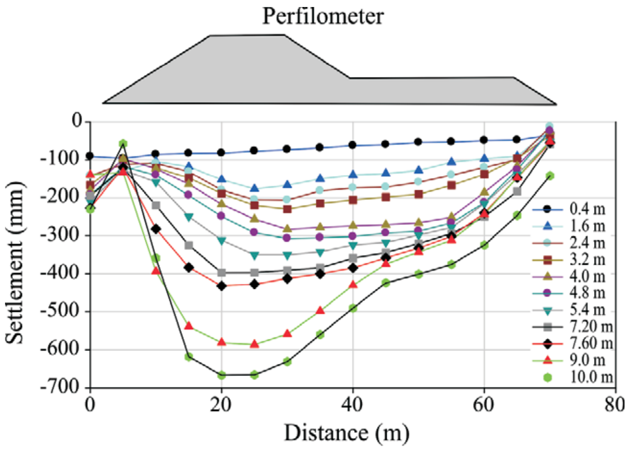


**Figure 37** - Results from the settlement profiler.

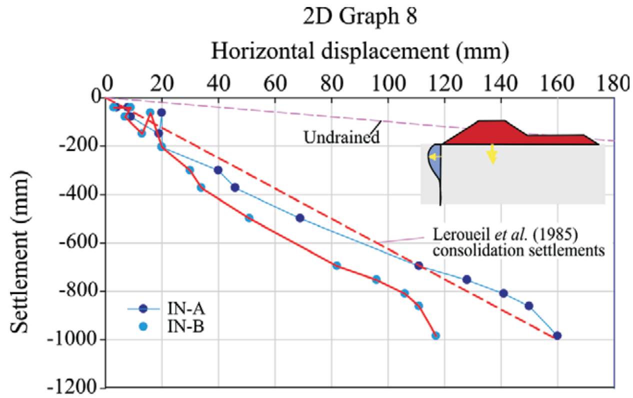


**Figure 38** - Relationship of settlements and horizontal displacements.

nometer distortions are especially useful for this purpose, as discussed long ago by Ortigao *et al.* (1983a, 1983b). Jumps in readings indicate that failure is approaching.

In addition to inclinometers, the only useful instrument to indicate impending failure, is a piezometer, but never as clear as inclinometer data.

Hunter & Fell (2003) analysed 13 case histories of embankment of soft soils and suggested that the following observations can be a good indication of imminent failure of embankment foundations: (a) lateral displacement at the embankment toe; vertical deformation at or just beyond the toe; (c) inclinometer observations at the toe; (d) embankment cracking and (e) porepressure behaviour.

Past experience with a few embankments on soft clay in Brazil (Ortigao *et al.*, 1983a,1983b, Ortigao, 1991) has led the authors to rely mainly on inclinometer data followed by piezometers. Surface marks yield useless data for failure prediction in most cases.

## 6. Stability Analyses

Limit equilibrium stability analyses were carried out to evaluate the strength of the tailings at the end of construction with Bishop's simplified method and circular slip surfaces. The Slide 5 computer program was used. The embankment fill parameters were set as $\gamma = 17$ kN/m$^3$, $c = 0$ and $\phi = 30^{\circ}$.

### 6.1. TSA total stress analyses

The tailings parameters varied according to the analysis case. Firstly, total stress analyses (TSA) were carried out with undrained strength assumptions for the tailings. The tailings parameters were $\gamma = 17$ kN/m$^3$ and the undrained cohesion and friction were taken as $c_u = 0.1\ \sigma'_v$, $\phi_u = 0$, as suggested in Morgenstern (2002) report and used in stability analyses of the dam. This resulted in FS = 0.171 (Fig. 39), which is too low.

A search was then conducted to check which undrained strength value would yield a FS just above 1, for end of construction conditions. The ratio $c_u/\sigma_v$ was increased until FS was just above one. Figure 40 presents the results which yielded $c_u/\sigma_v = 1.4$.

### 6.2. ESA effective stress analyses

The ESA consisted of a sensitivity analysis of FS as a function of the porepressure parameter $B$. The effective friction angle for the tailings was taken as $\phi' = 32°$. The ESA analyses were run varying $B$. Figure 41 presents the results which shows that FS = 1 for $B$ in the order of 0.9. This value is higher than observed at the end of construction, which was in the order of 0.5 to 0.7, which, in turn, would yield a FS value of about 1.2 to 1.3.

## 7. Discussion

The outcome of stability analyses is that TSA was unable to predict the embankment behaviour. The reason is clear: drainage. Indeed, Fig. 29 shows that all excess porepressures dissipated within 10 days after the end-of-construction. Therefore, a considerable amount of drainage took place during construction, despite a placement rate, which was as fast as possible, but still not sufficient to impede drainage.

ESA with porepressure parameter $B = 0.9$ yields FS close to one. Therefore, assuming that at the end-of-construction FS might have been close to 1.2-1.3, based on actual porepressure measurements, it is concluded that ESA is the only possible way to analyse stability.

## Conclusions

This field experiment has led to the following conclusions:

- The gold mine tailings behave like a loose silt material. Undrained triaxial tests on loose specimens show static liquefaction taking place under low confining stresses.
- Just after placing the first embankment layer, water and tailings surged through the fill. This phenomenon can be interpreted as static liquefaction taking place at low confining stress, as also observed in the triaxial tests.

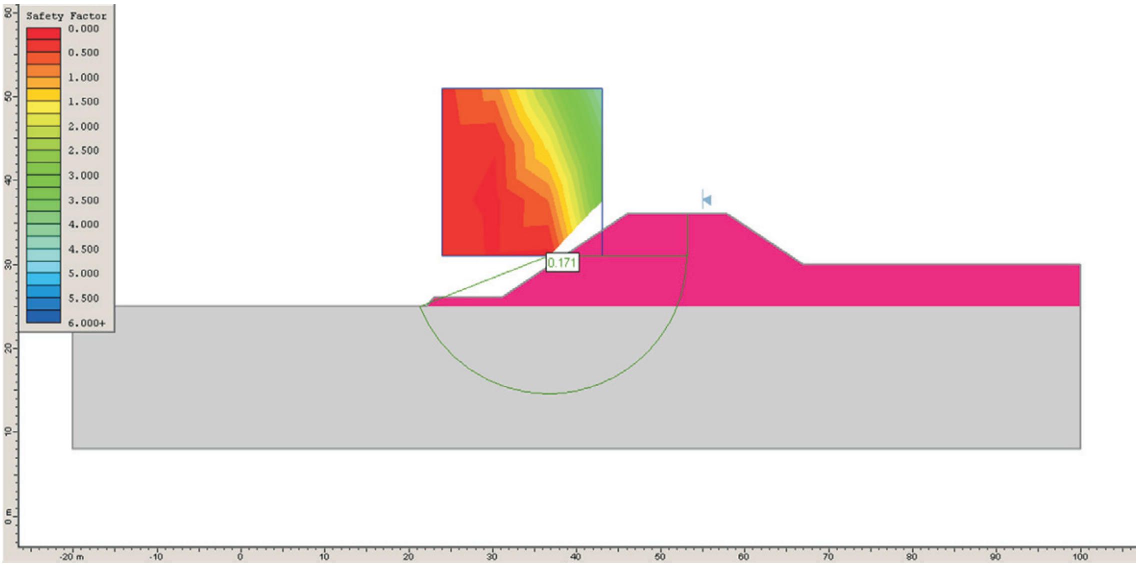


**Figure 39** - TSA stability analyses with $c_u = 0.1\ \sigma'_v$ yielding FS = 0.171.

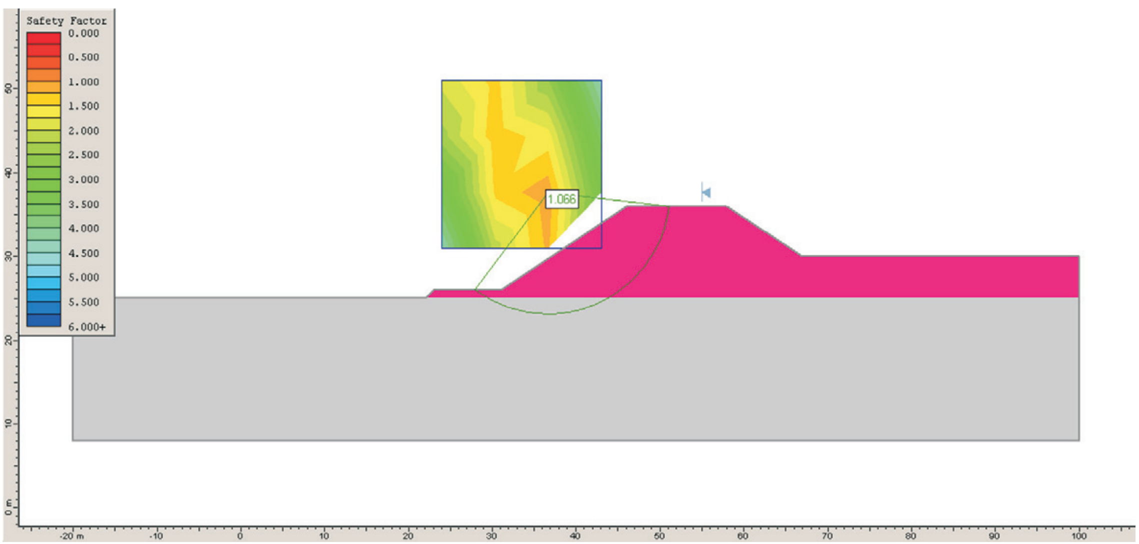


**Figure 40** - TSA stability analyses with $c_u = \sigma'_v = 1.4$, yielding FS = 1.066.

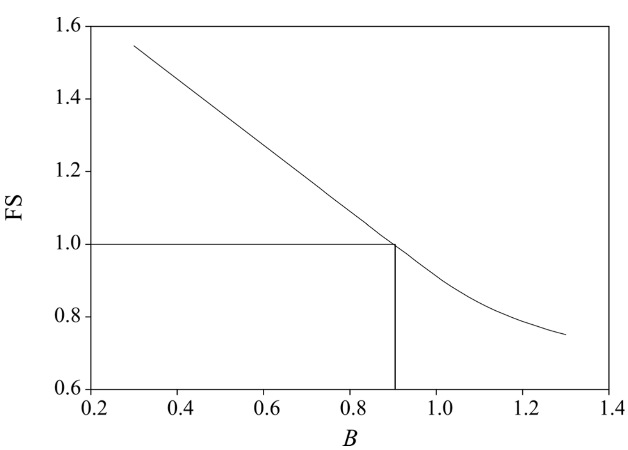


**Figure 41** - ESA sensitivity analyses, FS *vs.* B.

- Local yielding and lateral bulging at the tailings took place when the embankment reached 5 m height. This was clearly observed at the inclinometer IB and affected measured porepressures in all piezometers, which showed a small, but sharp porepressure drop, followed by recovery.
- At the end of construction the embankment was stable without any visible cracks or large visible deformation;
- The performance of the instrumentation was very good, yielding a large amount of accurate and reliable data;
- The construction rate was fast enough to yield high porepressure built-up in the tailings, followed by fast dissipation rates after the end of construction;

- Porepressure dissipation analyses showed that the coefficient of consolidation agrees well with piezocone dissipation test results;
- Back-figured TSA analyses at the end of construction yielded a very high undrained strength ratio of about 1.4, much higher than any other method based on CPTU and laboratory values. None of the undrained strength methods were able to predict the embankment behaviour.
- Effective stability analyses with estimated porepressure parameter *B* values indicated that failure would take place with *B* close to 0.9. This is by far larger than measured values at the end of the construction, which, in turn, shows a FS value in the order of 1.2-1.3. Therefore, the authors conclude that effective stress analyses is the only way to analyse stability on these tailings.

## Acknowledgments

The decision to carry out this experiment was supported by RPM mine geotechnical consultants: Mr S. Cale, Scott Wilson Mining Ltd, Mr D. Welch, Golder Associates and Mr B. Brown from Rio Tinto Mining. Dr S. Teixeira supervised the tests at the University of São Paulo, São Carlos Campus soils laboratory. Cimcop Contractors carried the earthworks. Mr John Ioannides from Geologismiki provided valuable software support. Dr M. Jefferies and Professor P.K. Robertson kindly reviewed the manuscript and gave many suggestions. To all the authors express our gratitude. RPM's permission to publish these results is kindly acknowledged.

## References

Byrne P, Puebla H, Chan DH, Soroush A, Morgenstern NR, Cathro DC, Gu WG, Phillips R, Roberston PK, Homan BA, Wride C, Sego D, Plewes HD, List BR & Tan S (2000) CANLEX full-scale experiments and modelling. Canadian Geotechnical Journal, v. 37, p. 543-562.

Leroueil S, Magnan JP & Tavenas F (1985) Remblais sur argilles molles, LCPC Laboratoire Central des Ponts et Chaussées et Technique et Documentation Lavoisier, Paris, 342 pp.

Hunter G & Fell R (2003) Prediction of impending failure of embankments on soft ground. Canadian Geotechnical Journal, v. 40, p. 209-220.

Jefferies M & Been K (2006) Soil Liquefaction: A Critical State Approach. Taylor & Francis, 479 pp.

Morgenstern N (2002), Review and Sign-off Report, Mina do Ouro Dam. RPM Unpublished Report, 2002.

Olson, SM & Stark, TD (2002) Liquefied strength ratio from liquefaction flow failure case histories. Canadian Geotechnical Journal, v. 39, p. 629-647.

Olson SM & Stark TD (2003) Yield strength ratio and liquefaction analysis of slopes and embankments. ASCE Journal of Geotechnical and Geoenvironmental Engineering, ASCE, v. 129:8, p. 727-737.

Ortigao JAR (1995) Soil mechanics in the light of critical state theories. AA Balkema, Rotterdam, 299 pp.

Ortigao JAR, Werneck MLG & Lacerda WA (1983a) Embankment failure on Rio de Janeiro clay. ASCE Journal of Geotechnical Engineering, v. 109:11, p. 1460-1479.

Ortigao JAR, Lacerda WA & Werneck MLG (1983b) The behaviour of the instrumentation of an embankment on clay, Proc. Int. Symp. on Field Measurements in Geomechanics, Zürich, Balkema, v. 1, pp. 703-707.

Ortigao JAR (1991) Embankment failures on soft clay in Brazil. Geotechnical News, v. 9:4, p. 68-70.

Roberson PK & Wride CE (1998) Evaluating cyclic liquefaction potential using the cone penetration test. Canadian Geotechnical Journal, v. 35, p. 442-459.

Robertson PK (2008) Discussion on Shuttle and Cunning (2007) Liquefaction potential of silts from CPTU. Canadian Geotechnical Journal, v. 45, p. 140-141.

Robertson PK (2009) Discussion on Boulanger and Idriss "Evaluation of cyclic softening in silts and clays", ASCE Journal of Geotechnical Engineering and Geoenvironmental Engineering, v. 135:2, p. 306-307.

Robertson PK (2010) Evaluation of flow liquefaction and liquefied strength using the CPT, ASCE Journal of Geotechnical and Geoenvironmental Engineering, v. 136:6, p. 842-853.

Robertson PK (2012) Guide to cone penetration testing, Gregg Drilling, www.greggdrilling.com.

Shuttle DA & Cunning J (2007) Liquefaction potential of silts from CPTU. Canadian Geotechnical Journal, v. 44, p. 1-19.

Yamamuro JA & Covert KM (2001) Monotonic and cyclic liquefaction of very loose sands with high silt content. Journal of Geotechnical and Geoenvironmental Engineering, v. 127:4, p. 314-324.

Yamamuro JA & Lade PV (1997) Static liquefaction of very loose sands. Canadian Geotechnical Journal, v. 34, p. 905-917.

Wride (Fear) CE, Robertson PK, Biggar KW, Campanella RG, Hoffmann BA, Hugues JM O, Küpper A & Woeller DJ (2000) Interpretation of in situ test results from the CANLEX site. Canadian Geotechnical Journal, v. 37, p. 505-529.